SPREADING OF WAXY OILS ON CALM WATER

Ute Brönner[a]*, Øistein Johansen[b], Frode Leirvik[a], Tor Nordam[a], and Kristin R. Sørheim[a]

[a] SINTEF Ocean AS, P.O. Box 4762, Torgard, 7465 Trondheim, Norway

[b] JOHANSEN ENVIRONMENTAL MODELING CONSULTING, Trondheim, Norway

* Corresponding author: ute.broenner@sintef.no

Abstract

The objective of this paper is to provide a simple extension of the much-used gravity spreading model for oil on calm water to account for the spreading behavior of waxy crude oils in cold waters – including the observed retardation and eventual termination of spreading at certain oil film thicknesses. This peculiar behavior is not predicted by traditional spreading models for oil on calm water (i.e. viscous-gravity spreading models), but may occur due to non-Newtonian oil properties caused by precipitation of wax at low temperatures. To clarify the spreading behavior of such oils, SINTEF has conducted a series of laboratory experiments with a range of waxy oil mixtures. The present paper contains analyses of data from these experiments, including favorable comparisons with calculations by a proposed improved surface spreading model.

Key Words

Surface oil, waxy crude oils, non-Newtonian behavior, oil spill modeling, gravity spreading

Introduction

The increased production of condensates and light crude oils on the Norwegian Continental Shelf, and the corresponding increased transport of condensates, crude oils and refined oil products along the coast, turned the attention towards these petroleum products in oil spill contingency planning in Norway. It has been assumed so far that the oil films formed by these oils are too thin for effective recovery, and that their life time on the sea surface is very short due to a high rate of evaporation, natural dispersion, and dilution in the water. However, residues of some waxy condensates and crude oils show different spreading behavior, thickness distribution and a longer lifetime on the sea surface, presumably due to solidification and wax precipitation. In effect, these oils have not received significant attention in the oil spill research communities to date, but are recommended by e.g. Murphy et al. (2016) for further study, based on an extensive survey of oil spill literature since 1968.

While the thickness and spatial extent of the spilled oil are important parameters in oil spill contingency planning and environmental risk assessments of potential oil spills from offshore oil installations or ship accidents, uncertainties still exist in the modelling of the

processes that causes surface spreading of oil. Novel approaches have been proposed quite recently to account for observed long-term spreading behavior (Simecek-Beatty and Lehr 2017, Durgut and Reed 2017). In the present paper, we will focus on surface spreading of oil in the vicinity of the source which forms the starting condition for subsequent spreading processes. At this early stage, spreading is generally assumed to follow the law of gravity spreading as developed by e.g. Fay (1969), Fanneløp and Waldman (1972) and DiPietro and Cox (1975). All approaches describe three specific spreading regimes, i.e. gravity-inertia, gravity-viscous and interfacial tension-viscous (Wu 2013). The behavior within the three regimes has been observed in laboratory experiments, but in oil spill situations the gravity-viscous regime is assumed to be valid in the period important for oil spill response. Subsequently, other spreading processes will dominate, such as shear spreading caused by oil entrainment due to wave action and subsequent resurfacing of oil droplets, as well as Langmuir circulation and horizontal oceanic diffusion (Reed et al. 1999). Our main objective here is to explain deviations between observations of short term spreading and predictions with common gravity spreading models, possibly related to mechanisms and oil properties not accounted for in these models.

In the commonly applied models for gravity spreading (or *gravity-viscous* to be more specific), the slope of the oil surface is supposed to be the driving force, while friction between the oil slick and the underlying water is the retarding force. Moreover, effects of oil viscosity are neglected based on the assumption that the viscosity of oil is large compared to the viscosity of water. The slope of the oil surface depends on the gradient in the film thickness and the density difference between water and oil. This implies that light oils (large density difference) will spread more rapidly than more heavy oils (smaller density difference).

Particularly viscous oils show retarded spreading velocities (relative to theory) and termination of spreading when a certain oil film thickness is reached (terminal film thickness). The existence of a terminal thickness has been acknowledged in oil spill models on an *ad hoc* basis by prescribing a certain terminal thickness for different oil types (Daling et al. 1997), or by assuming a correlation with oil viscosity (Venkatesh et al. 1990). As pointed out by Reed et al. (1999), the deviant behavior of retarded spreading velocities is most likely caused by certain mechanisms and/or oil properties not accounted for in the common spreading models. Such unaccounted mechanisms might be revealed in studies of related spreading phenomena, such as extensional thin layer flows as found in glass manufacturing (Howell 1994) and floating ice shelves (Pegler and Worster 2012), or spreading of viscoplastic fluids as in the formation of lava domes (Balmforth et al. 2004).

The purpose of the study presented in this paper has been to provide a simple extension of the present gravity spreading model for oil on calm water to account for the particular spreading behavior of waxy oils. This was accomplished by a new theoretical approach to the problem, backed up with some simple oil spreading experiments. The paper is organized in three main sections: the first is focused on spreading theory; the second

includes a brief description of the experimental setup; and the third contains a comparison between observed and computed oil spreading radii. The last section contains a summary of the findings. To make the paper more readable, we have included the most detailed model derivations in an Appendix.

Spreading theory

Theoretical equations for the spreading behavior of an oil slick can be derived from the force balance between spreading forces and retarding forces. Presuming that gravity is the dominating driving force, and friction between oil and water is the dominating retarding force, the bulk force balance can be written as

$$\frac{1}{2} h_0^2 \, \rho \, g' - R \, \mu_w \, U/\delta \; = 0 \, , \tag{1}$$

where h_0 (m) is the oil film thickness in the center of the slick, ρ and ρ_w (kg/m^3) are the density of oil and water, and $g' = g \, (\rho_w - \rho)/\rho_w$ (m/s^2) is the reduced gravity. In the second term R (m) is the radius of the slick, μ_w (N s/m^2)) is the dynamic viscosity of water, U (m/s) is the spreading velocity, and δ (m) is the boundary layer thickness in the water under the slick. With the latter expressed by the Blasius formula for flow around a flat plate, i.e. $\delta \sim \sqrt{\nu_w X/U}$, and replacing U with dR/dt, we arrive at the following differential equation for the slick radius:

$$\frac{d}{dt} R^{4/3} = c \, (h_0^2 \, \rho \, g')^{2/3} (\rho_w \mu_w)^{-1/3}, \tag{2}$$

where c is a constant to be determined empirically.

For axisymmetric spreading with a time varying oil volume $V(t)$ (m^3), the central film thickness h_0 will be linked to oil volume and slick radius by the equation

$$f h_0 \pi \, R^2 = \, V(t), \tag{3}$$

where the factor $f \leq 1$ depends on the oil slick thickness profile, with $f = 1$ for a constant film thickness (see Appendix for more details). With a constant oil discharge rate q (m^3/s), the oil volume can be written as $V(t) = q \, t$. By substituting h_0 from Eq. 3 into Eq. 2 and integrating, we get the following expression for the slick radius for radial spreading with a constant oil rate:

$$R = c' \, (q^2 \rho g')^{1/6} \, (\rho_w \mu_w)^{-1/12} \, t^{7/12} \, , \tag{4}$$

where c' is an aggregated constant of proportionality in the order of 1.

The rationale for neglecting the effect of oil viscosity in the gravity spreading model is that the viscosity of crude oils is generally much larger than the viscosity of water. Under such conditions, the vertical velocity gradient in the oil layer will be small, and the layer will spread as a slab. Since high oil viscosity is an implicit assumption in the gravity spreading model, further increase in oil viscosity will not affect the spreading rate (see Appendix for

details), as well as oils with different viscosities but similar densities will follow the same spreading regime.

For high viscosity oils, a second resisting force could be of importance, i.e. the force related to stretching of the oil film. Uniaxial stretching will generate a retarding force $F = \sigma_n A$, where A is the cross-sectional area of the oil slick, and σ_n is the normal stress given by the relation $\sigma_n = \mu_E \dot{\varepsilon}$, where μ_E (Ns/m^2) is the *elongational viscosity* of the oil, and $\dot{\varepsilon} = U/L$ (s^{-1}) is the rate of strain, where U (m/s) is the velocity at the front of the slick and L (m) is the length of the slick. For Newtonian fluids, the elongational viscosity is known to be three times the shear viscosity (Trouton's ratio), i.e. $\mu_E = 3\mu$. If this retarding force is included in the force balance equation (Eq. 1), the effect is found to be negligible in most cases. Moreover, the equation also shows that adding a force caused by the elongational velocity of a Newtonian fluid will only slow down the spreading rate but not cause spreading to terminate (see Appendix for details).

For non-Newtonian fluids, a finite stress is required to move the oil from rest. For so-called Bingham fluids, the shear stress τ (Pa = N/m^2) is given by $\tau = \sigma_Y + \mu_P \dot{\gamma}$, where σ_Y (Pa) is the yield stress, μ_P (N s/m^2) is the plastic viscosity, and $\dot{\gamma}$ (1/s) is the shear rate. For Newtonian fluids, the yield stress is zero by definition, and $\mu = \mu_P$ independent of the shear rate. The elongational stress for Bingham fluids is given by a similar equation, with the plastic viscosity being 3 times the shear related plastic viscosity for a specific shear, and the elongational yield stress being $\sqrt{3}$ times the shear related yield stress (see Appendix).

As explained in more detail in the Appendix, including this in the force balance equations implies that for oil with significant yield stress, spreading will be retarded by the elongational force, and eventually come to a stop when the oil reaches a terminal film thickness h_∞. This thickness is a result of a balance between the gravity induced spreading force and the retarding force imposed by the yield stress, implying

$$h_\infty = 2\,\sigma_{YE}/(\rho\, g'), \qquad (5)$$

where σ_{YE} (N/m^2) is the elongational yield stress.

Including only the yield stress term in the elongational retarding force of the spreading equation, equation 2 can be expressed as:

$$\frac{d}{dt} R^{4/3} = c\,(h_0^2 \rho\, g' - 2h_0\sigma_{YE})^{2/3}(\rho_w \mu_w)^{-1/3}, \qquad (6)$$

where the term $h_0^2 \rho\, g' - 2h_0\sigma_{YE}$ should be replaced by zero when its value becomes negative. Note that with a yield stress measured under shear stress conditions (i.e. as σ_Y), $\sigma_{YE} = \sqrt{3}\sigma_Y$.

Eq. 6 will be used in the following analysis of the results from the spreading experiments reported in the next section.

Spreading experiments

The spreading experiments were designed to simulate radial spreading of oil released continuously on calm water. The choice of continuous releases was partly based on preliminary experiments with instantaneous releases of a constant volume of oil (1 L), which showed spreading behavior in the gravity-inertia regime, rather than in the gravity-viscous regime we wanted to investigate (unpublished results). Since the spreading theory indicates that the duration of the gravity-inertia regime is significantly shorter for continuous releases, we decided to use a continuous discharge in the present experiment. In order to cover a controlled range of non-Newtonian behavior, i.e. in yield stress values, the experiments were performed with model oil made from mixtures of two oils with low and high wax content, respectively: Wide Range Diesel (WRD) and artificially weathered Norne crude (Norne 250+). The two oils have the approximately same density and would show the same spreading behavior according to classic spreading theory. Additionally, the oils were supposed to exhibit minor changes in properties due to evaporation for the duration of the experiments (about 4 minutes). Thus, with almost equal density of the different blends of these oils, any differences in spreading behavior would be related to other effects, as e.g. yield stress effects.

The experiments were conducted in a circular basin with a diameter of 5.5 m and 1.3 m height. The basin was filled with sea water to a depth of 87 cm. The oil mixture was discharged in the center of the basin with a continuous pumping rate of 2 L/min for a period of 2 minutes. The discharge occurred through a funnel with a maximum diameter of 10 cm, located 2 mm below the water surface. Spreading of the oil was recorded at 0.5 s intervals for a period of about 4 minutes with a camera mounted about 4 m above the basin. The pictures were processed digitally to obtain areas within the slick corresponding to certain thickness intervals (e.g. 0.5 – 1mm, 1 – 2 mm, and > 2 mm). In order to establish a relation between oil film thickness and pixel intensity, additional measurements of the oil film thickness were obtained with an ultrasonic device (a 20 MHz focused transducer from Panametrics) during the constant volume phase of each experiment (Fig. 1). The transducer was mounted 2 cm below the water surface, and could be towed radially along a rail placed on the bottom of the basin.

Table 1 summarizes the properties of the various blends of Wide Range Diesel (100 % WRD) and the weathered waxy crude oil (Norne 250+) used in the spreading experiments. The density of the Wide Range Diesel is 894 kg/m^3, while Norne 250+ has a density of 888 kg/m^3. In addition, one experiment was performed with a Marine Gas Oil (MGO), with a density of 846 kg/m^3 and a negligible or minor yield stress. The yield stress values in the table are given based on two different methods, i.e. values obtained from an oscillating rheometer, and values based on curve fit of data from a rotating rheometer to a Bingham fluid model. A curve fit of shear stress vs. shear rate for the 30 % blend of Norne 250+ in WR is shown as an example in Figure 2, but similar near Bingham fluid behavior was found for the other blends. Differences between the two methods are notable, as well as some apparent deviations from a monotonous increase in yield stress with increasing fractions of Norne 250+ in the blends. The former discrepancy may be an effect of

different accuracy in the methods, while the latter effect might be explained by inconsistencies in sample preparations (uneven mixing) prior to the measurements.

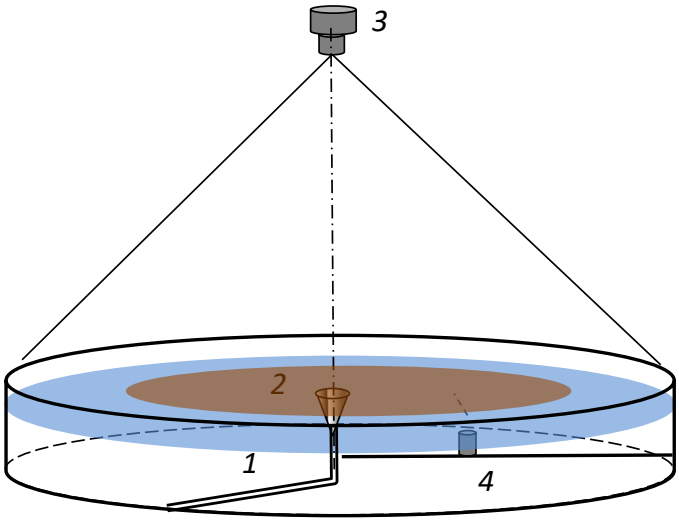

Figure 1. Principal sketch of test basin (5.5 m Ø, 87 cm water depth) used for the oil spreading experiments. The numbers indicate the pumping line for oil with the discharge funnel at the top (1), the oil slick spreading on the water surface (2), the recording camera (3), and the ultrasound device for thickness measurements (4). The ultrasound device was towed along a rail mounted at the bottom of the basin.

Table 1. Properties of the oil mixtures used in the experiments. Oil was released at a rate of 2 L/min for a period of 2 minutes. MGO is a marine gas oil, WRD is a wide range diesel, and the blends are mixtures of WR and Norne 250+.

			Fraction of Norne 250+ in mixture			
Blend	MGO	WRD	5 %	10 %	20 %	30 %
Density (kg/m^3)	846	894	894.1	893.7	893.1	892.4
Yield Stress (Pa):						
Oscillating rheometer	0	0.36	1.25	0.46	1.65	13.6
Bingham model fit	0	0.75	1.45	1.32	2.95	44.6

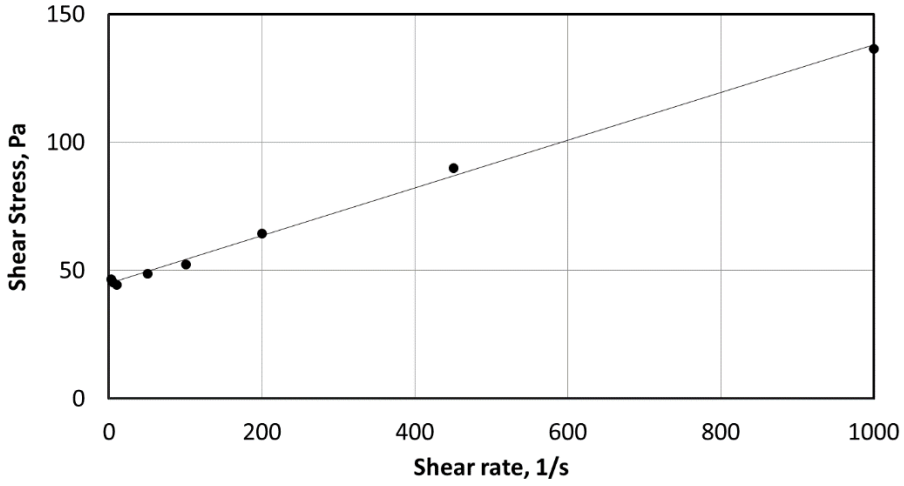

Figure 2. Plot of shear stress vs. shear rate for 30 % Norne 250+ in Wide Range Diesel. The straight line is a Bingham fluid fit to the data.

Observed spreading and comparisons with model predictions

The digital processing of the images from the experiments gave equivalent radii for a set of thickness classes, but did not provide the full radial extension of the slick that is required for comparisons with model predictions. As explained in the Appendix, we have made use of the oil thickness profiles we obtained from the ultrasonic device during the stagnant phase of the experiments to obtain such data. Figure 3 shows equivalent radii (of perfect circles) obtained from the areas recorded for the different thickness classes from one experiment with Wide Range Diesel (Exp. 12). The vertical red line marks the duration of the release. The full radius of the slick that was derived from these data is shown as a broken line. Figure 4 shows full radial extents estimated in the same way based on data from experiments with different blends of Norne 250+ in Wide Range Diesel, in addition to one experiment with a lighter Diesel oil.

Figure 4 shows that the spreading of the lighter Diesel oil (Exp. 18) continues after pumping is stopped (red vertical line at 120 s), while the estimated radial extent for the various blends of Norne 250+ in Wide Range Diesel show a distinct termination of spreading after this time, and at smaller radii with increasing fractions of Norne 250+. This termination is a strong indication of a yield stress effect (Eq. 5), implying increased terminal film thickness with increased yield stress.

Results obtained after release end are summarized in Table 2 for all experiments with blends of Norne 250+ and Wide Range Diesel. The full spreading radius and the corresponding central thickness are obtained at 180 s from the start of the experiment, i.e. 60 seconds after the release was stopped. Note that experiments 11, 12, and 13 are replica with Wide Range Diesel, while experiments 15, 16 and 17 are replica with blends of 20 % Norne 250+.

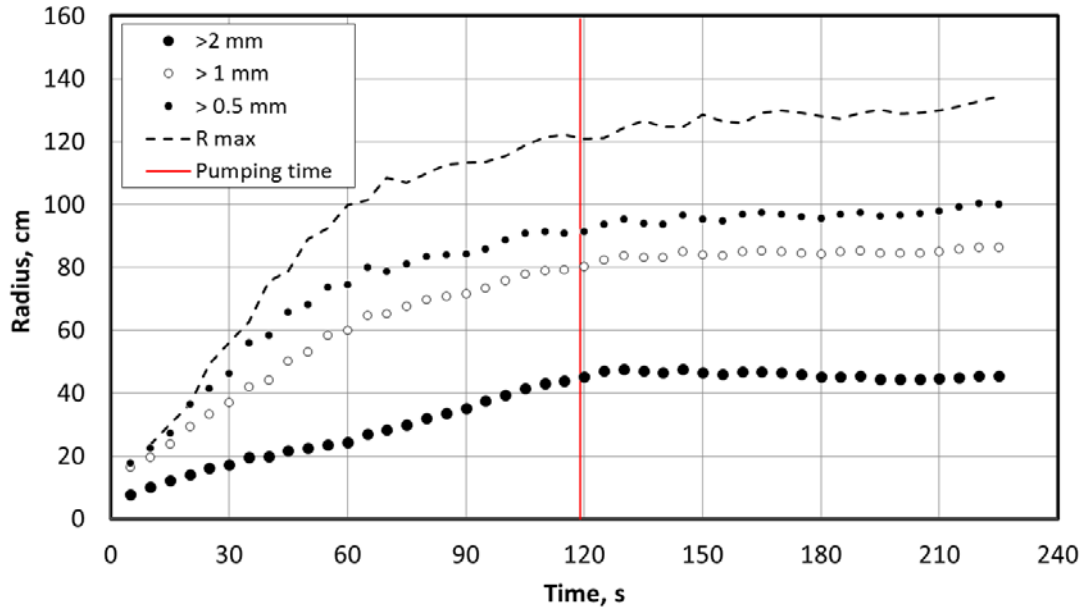

Figure 3. Equivalent slick radii for three different oil film thickness classes (> 0.5 mm, 1 mm, and 2 mm) obtained from the experiment with Wide Range Diesel (Exp. #12). The broken line marked "R max" shows the estimated full radial extent of the slick (see text). The vertical red line shows the release time in the experiment.

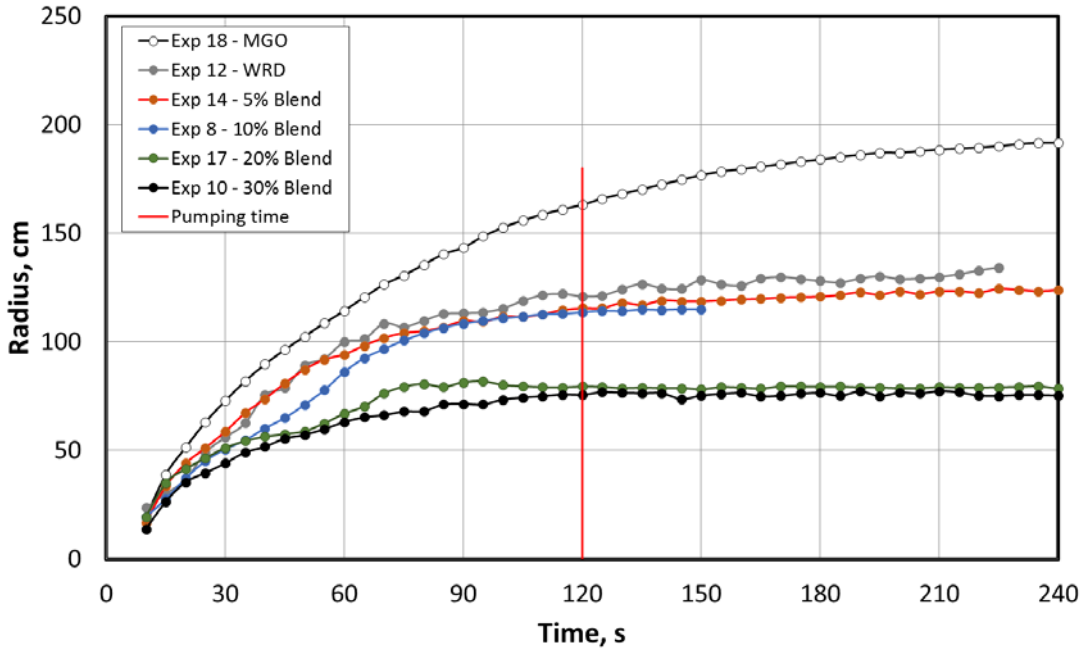

Figure 4. Estimated radial extent for a Marine Gas Oil (MGO) and various blends of Norne 250+ in Wide Range Diesel (WRD). The full radial extent is estimated from observed equivalent radii for three thickness classes, and an assumed thickness profile (see Appendix).

Table 2. Terminal spreading radius and central film thickness (h_0) determined from spreading experiments with different blends of Norne 250+ in Wide Range Diesel (WRD).

The yield stress values are from Table 1, based on data obtained with the oscillating rheometer.

Experiment	Blend	Yield stress, Pa	Radius, cm	h_0, mm
8	10 % Norne	0.46	115	4.8
10	30 % Norne	13.6	77	5.7
11			122	2.1
12	WRD	0.36	128	1.9
13			127	2
14	5 % Norne	1.25	121	2.2
15			77	5.4
16	20 % Norne	1.65	71	6.5
17			79	5.1

The results in Table 2 and Figure 4 show a tendency towards reduced terminal radii and increased terminal thicknesses with increasing fractions of Norne 250+, but no clear effect is observed for the last increase from 20 to 30 % Norne 250+. The latter may be an effect of loss of coherence (breakup) of the nearly rigid oil film, as seen on the picture from the experiment with 30 % Norne 250+ (Figure 5).

Figure 6 shows spreading radii computed with the modified spreading model (Eq. 6) for a range of yield stresses from 0 to 2 Pa (see labels), compared with the observed spreading radii from the experiments with different blends (also shown in Figure 6). The computations were made by numerical integration of Eq. 6 with the empirical constant chosen as c = 1.5. For each time step, the following computations are made:

a) $h_n = V_n/(f\ \pi\ R_n^2)$,

where R_n and V_n are the slick radius and released oil volume at time step n,

b) $R_{n+1}^{4/3} = R_n^{4/3} + 1.5 \times (\rho_w \mu_w)^{-1/3}\ \times\ F_s^{2/3} \times\ \Delta t$,

where $F_s = Max\left(h_n^2\ \rho\ g' - 2\ h_n \sigma_{Y,E}, 0\right)$ is the spreading potential.

c) $R_{n+1} = \left(\ R_{n+1}^{4/3}\right)^{3/4}$

This procedure requires an initial value for R, which may be obtained from an analytical expression of radial spreading (e.g. Eq. (4) or a corresponding equation from Chebbi, 2014).

The favorable agreement between the computed spreading for the low yield stress oils (solid lines marked with 0 and 0.25 Pa in Figure 6) and the observed spreading of the low yield stress Marine Gas Oil (MGO) is a strong indication for a gravity-viscous dominated spreading behavior we wanted to achieve with the choice of continuous releases of oil.

A closer inspection of the results in Figure 6 shows that the main deviations between observed and computed radii are found for the largest yield stresses, where the reduction in the terminal radius levels off in the experiments, while the model predicts a continuing reduction in the terminal radius with increasing yield stress. However, it is possible that the observed off-leveling may be caused by the breakup of the nearly rigid oil at high yield stresses. Accounting for this effect and the uncertainty in the estimate of the full spreading radius, the relatively large uncertainties in the determination of yield stress, and the simplifications in the model, the trend in the computed spreading with increasing yield stress are found to compare favorably with the trend in the spreading observed in the experiments.

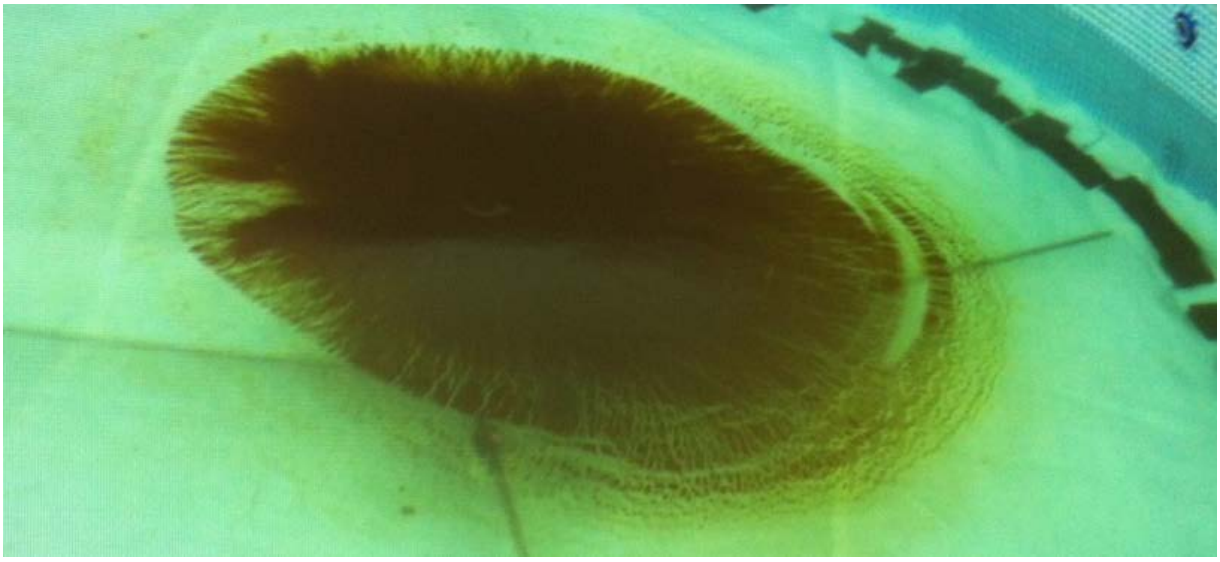

Figure 5. Picture from the spreading experiments with a blend of 30 % Norne 250+ in Wide Range Diesel.

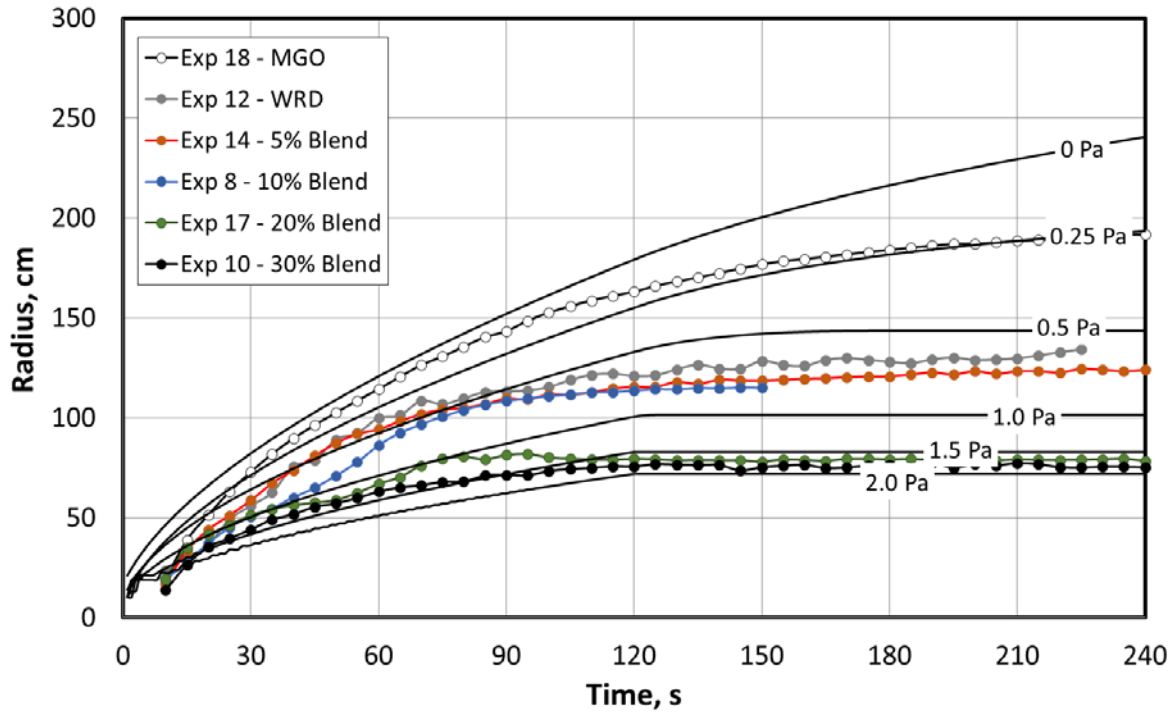

Figure 6. Observed and computed radial spreading. Lines with markers represent observed spreading radii for different blends (same as in Fig. 4), while lines with labels are computed spreading radii for a range of yield stresses from 0 to 2 Pa (see labels).

Summary and conclusion

Waxy oils may show non-Newtonian rheological properties due to precipitated wax-components, particularly after weathering. In order to clarify the effect of such properties on the spreading behavior, a series of laboratory experiments have been conducted by SINTEF with waxy oil mixtures. In the present paper, data from these experiments have been compared with calculations based on a modified surface spreading model. In the proposed model (Eq. 6), an elongational stress related to the yield stress is included as a retarding force opposing the spreading force due to gravity. When these forces balance, the oil slick will reach its terminal thickness (Eq. 5).

Presently, nine successful experiments, including some replica, have been conducted (Table 2), one with an MGO Diesel oil, and 8 with different blends of Wide Range Diesel (WRD) and Norne 250+ (Table 1). The results from these experiments were reported as a set of equivalent radii, each related to a certain thickness category derived from image analyses of pictures from the experiments. Based on ultrasound thickness measurements in the stagnant phase of the experiments, a general thickness profile was estimated (see Appendix). On this basis, the full spreading radius was estimated for each experiment based on the combination of thickness classes and radii (Figures 3 and 4).

Spreading radii were computed with the modified spreading model (Eq. 6) for a range of yield stresses from 0 to 2 Pa. Accounting for the simplifications in the model, and the relatively large uncertainties in the determination of yield stress, the trend in the

computed spreading with increasing yield stress were found to compare favorably with the trend in the spreading observed in the experiments (Figure 6).

On this basis, we recommend that the new model should be included in operational oil drift and fate models, replacing ad hoc estimates of terminal film thickness. However, in order to facilitate this, yield stress data must be available for the oils under consideration, both in fresh state and at various degrees of weathering. Operational oil spill models account for changes in viscosity and implement a numerical model for the development of viscosity due to ambient sea temperature and oil weathering, as evaporation and water uptake (Johansen, 1991; Reed et al., 1999). To develop this kind of model for the development of yield stress is a major challenge, as long as such data are not reported regularly.

Acknowledgements

The present paper is based on results obtained as part of a competence and knowledge building project within the Research Council of Norway (RCN) PETROMAKS2 program.

The project "Thin Oil Films - Formation and behavior of thin oil films and evaluation of response methods including HSE" (233981/E30) was supported by the RCN and the oil companies Aker BP, Centrica, Eni, ENGIE, Shell, Statoil and Total through this program.

The authors are grateful for the support received from this project.

We also want to thank the reviewers for helpful comments and corrections to the manuscript.

References

Balmforth, N.J., R. V. Craster and R. Sassi, 2004: Dynamics of cooling viscoplastic domes. J. Fluid Mech., 499, 149–182

Chebbi, R., 2014: Viscous-Gravity Spreading of Oil on Water: Modeling and Challenges. Int. J. Chem. Eng. and Applications, 5, 186-189.

Daling, P. S., O. M. Aamo, A. Lewis, and T. Strøm-Kristiansen, 1997: SINTEF/IKU oil weathering model: Predicting oils' properties at sea. Int. Oil Spill Conference Proc. 1997, 297-307.

Di Pietro, N. D. and R. G. Cox, 1979: The spreading of a very viscous liquid on a quiescent water surface. Q. J. Mechanics & Appl. Math., 32, 355-381.

Durgut, I. and M. Reed, 2017: Modeling of spreading of oil slicks based on random walk and Voronoi diagrams. Marine Pollution Bulletin, 118, 93-100.

Fanneløp, T.K. and G. D. Waldman, 1972: Dynamics of oil slicks. AIAA Journal, 10, 506-510.

Fay, J.A., 1969: The spreading of oil on a calm sea. In D. Hoult (Ed.), Oil on Sea, Plenum Press, 114 pp.

Howell, P.D., 1994: Extensional Thin Layer Flows. Ph.D. Thesis, St. Catherine's College, Oxford, 150 pp.

Huppert, H, 1982: The propagation of two-dimensional and axisymmetric viscous gravity currents over a rigid horizontal surface. J. Fluid Mech, 121, 43-58.

Johansen, Ø., 1991. Numerical Modelling of Physical Properties of Weathered North Sea Crude Oils. DIWO-report No. 15, SINTEF IKU-report 02.0786.00/15/91.

Martinie, L, H. Buggish, and N. Willenbacher, 2013: Apparent elongational yield stress of soft matter. J. Rheol. 57, 627-646.

Murphy, D. et al., 2016: An in-depth survey of the spill literature since 1968: Long term trends and changes sin Deepwater Horizon. Marine Pollution Bulletin, 113, 371-379.

Nihoul 1984. Quoted by Deleersnijder, E., 1992: Revisiting Nihoul's model for oil slicks transport and spreading on the sea. Ecological Modelling, 64, 71-75.

Pegler, S.S and Worster, M.G.., 2012: Dynamics of a viscous layer flowing radially over an inviscid ocean. J. Fluid Mech., 696, 152-174.

Reed, M., Ø. Johansen, P.J. Brandvik, P. Daling, A. Lewis, R. Fiocco, D. Mackay and R. Prentki, 1999: Oil Spill Modeling towards the Close of the 20th Century: Overview of the State of the Art. Spill Science & Technology Bulletin, 5, 3-16.

Simecek-Beatty, D., and W. J. Lehr, 2017: Extended oil spill spreading with Langmuir circulation. Marine Pollution Bulletin, 122, 226-235.

Venkatesh, S., H. El-Tahan and R. Abdelnour, 1990: Modeling of the behavior of oil spills in ice-infested waters. Atmosphere-Ocean, 28, 303-329.

Wu, Z., 2013: A comment on Fay's formulae about spreading of oil slick on water surface. Applied Mechanics and Materials, 420, 259-262.

Appendix

Effects of oil viscosity

As stated in the main text, the rationale for neglecting the effect of oil viscosity in the gravity spreading model is mainly that the viscosity of crude oils is generally much larger than the viscosity of water. Under such conditions, the vertical velocity gradient in the oil layer will be small, and the layer will spread as a slab. This can be found by equating the shear stresses at the oil-water interface, i.e. $\tau_{water} = \tau_{oil}$, where:

$$\tau_{water} = \mu_w \left.\frac{\partial u}{\partial z}\right|_{water} = \mu_w \frac{U_b}{\delta},\ \tau_{oil} = \mu \left.\frac{\partial u}{\partial z}\right|_{oil} = \mu \frac{U_t - U_b}{\beta\, h}. \tag{A1}$$

Here, U_t and U_b are the spreading velocities at the top and bottom of the oil slick, μ and μ_w are viscosities of oil and water, δ is the boundary layer thickness in the water below the slick, h is the local oil film thickness, and $\beta < 1$ is a factor depending on the velocity profile in the oil. For the analogue case of viscous gravity spreading over a rigid surface, $\beta = 0.5$ (Huppert 1982).

Equating the two shear stresses gives

$$U_t = U_b \left(1 + \frac{\mu_w}{\mu}\frac{\beta h}{\delta}\right) \tag{A2}$$

For $\mu \gg \mu_w$ and/or $\delta \gg \beta h$ the last term in the parenthesis will be negligible, and the velocity difference will vanish. This implies, that since high oil viscosity is an implicit assumption in the gravity spreading model, further increases in oil viscosity will not affect the spreading rate.

For high-viscosity oils, a second resisting force may be of importance, i.e. the force related to stretching of the oil film. Uniaxial stretching will generate a retarding force $F = \sigma_n A$, where A is the cross-sectional area of the oil slick, and σ_n is the normal stress given by the relation

$$\sigma_n = \mu_E \dot{\varepsilon}. \tag{A3}$$

In this equation, μ_E (Ns/m^2) is the *elongational viscosity* of the oil, and $\dot{\varepsilon} = U/L$ (s^{-1}) is the rate of strain, where U (m/s) is the velocity at the front of the slick and L (m) is the length of the slick.

For Newtonian fluids, the elongational viscosity is known to be three times the shear viscosity (Trouton's ratio), i.e. $\mu_E = 3\mu$. Including this in the force balance equation (Eq. 1 in the main text), we find

$$\frac{1}{2} h_0^2\, \rho\, g' = R\, \mu_w \frac{U}{\delta} + 3\mu\, h\, \frac{U}{R} \equiv R\, \mu_w \frac{U}{\delta}\left[1 + 3\frac{\mu}{\mu_w}\frac{h\delta}{R^2}\right] \tag{A4}$$

With both h and δ will be small compared to R, the new resisting term will be orders of magnitude smaller than the oil/water friction term, and thus negligible in most cases. Moreover, the equation also shows that adding a force caused by the elongational velocity

of a Newtonian fluid will only slow down the spreading rate, but not cause the spreading to terminate.

For non-Newtonian fluids, a finite stress may be required to move the oil from rest. For so-called Bingham fluids, the shear stress τ (N/m^2) is given by

$$\tau = \sigma_Y + \mu_P \dot{\gamma} \quad \text{(A5)}$$

where σ_Y (N/m^2) is the yield stress, μ_P (N s/m^2) is the plastic viscosity, and $\dot{\gamma}$ (1/s) is the shear rate. For Newtonian fluids, the yield stress is zero by definition, and $\mu = \mu_P$ independent of the shear rate. The elongational stress for Bingham fluids is given by the following equation (Martinie et al. 2013):

$$\sigma_n = \sigma_{Y,E} + \mu_{PE}\dot{\varepsilon}, \quad \text{(A6)}$$

where σ_{YE} is the elongational yield stress, and μ_{PE} is the corresponding plastic viscosity. For this type of fluid, $\sigma_{YE} = \sqrt{3}\sigma_Y$ and $\mu_{PE} = 3\mu_P$, where σ_Y and μ_P are the corresponding shear stress values (Eq. A5).

This implies that for waxy oils where the yield stress may be significant, the spreading will be retarded by the elongational force, and eventually come to a stop when the oil reaches a terminal film thickness h_∞. This thickness is a result of a balance between the gravity induced spreading force and the retarding force imposed by the yield stress:

$$\frac{1}{2}h^2 \rho\, g' = h\, \sigma_{YE}, \text{ implying } \quad h_\infty = 2\, \sigma_{YE}/(\rho\, g'), \quad \text{(A7)}$$

where σ_{YE} (N/m^2) is the elongational yield stress.

Including only the yield stress term in the elongational retarding force, the spreading equation (Eq. 2 in the main text) can be expressed as:

$$\frac{d}{dt}R^{4/3} = c\,(h_0^2 \rho\, g' - 2h_0\sigma_{YE})^{2/3}(\rho_w \mu_w)^{-1/3}, \quad \text{(A8)}$$

where the term $h_0^2 \rho\, g' - 2h_0\sigma_{YE}$ should be set to zero when its nominal value becomes negative. Note that with a yield stress measured under shear stress conditions (i.e. as σ_Y),

$$\sigma_{YE} = \sqrt{3}\sigma_Y.$$

Oil film thickness profile

As mentioned in the main text, for axisymmetric spreading with a time variating oil volume $V(t)$ (m^3), the central film thickness h_0 will be linked to oil volume and slick radius R by the equation

$$f h_0 \pi\, R^2 = V(t), \quad \text{(A9)}$$

where the factor $f \leq 1$ depends on the oil slick thickness profile, with $f = 1$ for a constant film thickness. In general, however, the oil film thickness will vary with radial distance r from the center of the slick, from a maximum thickness $h = h_0$ at the center to $h = 0$ at the

leading edge of the slick (r = R). Assuming self-similarity, the thickness profile may be expressed in terms of a normalized distance $x = r/R$:

$$h(x) = h_0\,\varphi(x),\ 0 \le x \le 1 \qquad \text{(A10)}$$

For radial spreading of a fixed volume of oil on water, Nihoul (1984) proposed a normalized thickness profile $\varphi(x) = \left(1-(x)^2\right)^{1/2}$. The corresponding thickness at the center of the slick will then be $h_0 = 3/2\,V/(\pi R^2)$, implying f = 2/3 in Eq. A9. Other profiles (and f-values) may be relevant for cases with constant discharge rates and non-Newtonian fluids considered in this study.

Figure A1 shows thickness profiles obtained from three replicate experiments with Wide Range Diesel conducted in the study reported here. The radial distance and the oil film thickness are shown in normalized form in the plot, i.e. as φ vs. x_e, where $x_e = r/R_e$ and $\varphi = h/h_0$. The scaling radius R_e is an e-folding radius, corresponding to the radial distance where the thickness $h = h_0/\mathrm{e}$. The red curve shows a fitted function

$$\varphi(x_e) = \exp(-x_e^p) \qquad \text{(A11)}$$

where p = 3.5 is a fitted exponent.

Similar normalized thickness profiles were found from experiments with different mixtures of Wide Range Diesel and the Norne 250+ residue. For this normalized profile, the oil volume corresponding to a given e-folding radius and central oil film thickness will be given as

$$V = f_e\,h_0\,\pi\,R_e^2, \qquad \text{(A12)}$$

where $f_e = 2\int_0^\infty \varphi(x)\,x\,dx = 0.891$.

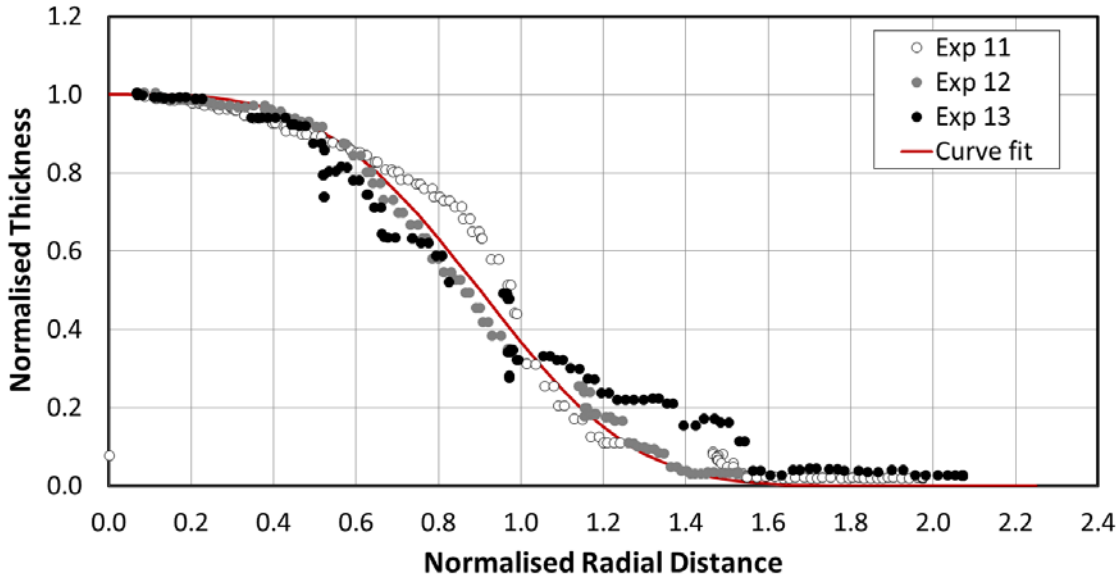

Figure A1. Thickness profiles obtained from experiments with Wide Range Diesel. The oil slick thickness is normalized by division by the central thickness, while the radial

distances are normalized by division with the e-folding radius R_e (see text). The red curve is a fitted super-Gaussian function (see text).

The normalized thickness profile given by Eq. A11 does not contain a final distance to the leading edge of the slick, but we have assumed that the leading slick edge is at a radius corresponding to R = 1.5 R_e, where the film thickness will be between 1 and 2% of the central film thickness. Inserted in Eq. A12, this gives

$$V = f\ h_0\ \pi\ R^2, \tag{A13}$$

where $f = f_e/1.5^2 = 0.396$

Eq. A13 was used in the comparison of computed spreading radii with observed spreading data.

Estimation of full radial slick extent

The recorded images of the spreading slick were processed digitally to obtain areas corresponding to different thickness classes. The areas A_i obtained for the different classes were converted to equivalent radii R_i of perfect circles by the relation $A_i = \pi\ R_i^2$.

In order to facilitate comparisons with spreading calculations, we need to define the full radial extent of the slick. With the assumption that the normalized thickness profile (Eq. A11) is generally valid, we can estimate the e-folding radius R_e from the radii R_i and R_j corresponding to two thickness classes h_i and h_j:

$$R_e^{(i,j)} = \left[\frac{R_j^p - R_i^p}{ln(h_i/h_j)}\right]^{1/p} \tag{A14}$$

With three thickness classes and three corresponding radii, estimates of R_e can be made for three combinations of film thickness (h_1, h_2, h_3) and radii (R_1, R_2, R_3). The mean of these estimates is used to establish the full radial extent of the slick, i.e.

$$R_e = \left(R_e^{(1,2)} + R_e^{(1,3)} + R_e^{(2,3)}\right)/3 \tag{A15}$$

As mentioned above, the full radial extent is assumed to be R = 1.5 R_e.